

Abstract

The model of compositionally layered mantle convection comprises a convectively isolated reservoir of several 100's of kilometers above the core. In this reservoir, a positive thermal buoyancy force counteracts a negative compositional buoyancy force. This thermo-chemical balance results in a layer that is stable, but that shows a convectively induced, time-varying topography.

In recent years, the model of compositionally layered mantle convection has become increasingly popular, due to indications from various fields of research. The model is able to explain constraints from geochemical and seismological studies and calculations on the Earth's heat budget. However, conclusive evidence, confirming the model, has not been found and a strong argument against compositional layering is the unsuccessful search for seismic reflections from a chemical interface.

In this study, numerical methods were adopted in order to examine the long-term dynamic behaviour of compositional layering in a cooling mantle. New aspects in this light are the incorporation of the 660-km phase transition and the simulation of heat exchange with the core. Four parameter tests were performed to investigate the sensitivity of the model. In order to compare the numerical calculations with seismological mantle constraints, lateral variations in seismic wave velocities were predicted, using a linear combination of the composition and temperature distribution.

From the numerical results it was concluded that compositional layering is dynamically stable over a model time comparable to the age of the Earth. A transition from layered to non-layered mantle convection occurs after ca. 2 Gyr, in which the phase transition plays a key role. At the end of the model time, after 4.5 Gyr, several quantities are in reasonable agreement with present-day Earth values. For the parameter space examined, the sensitivity tests show that the general characteristics of the model are robust. Finally, the predicted variations in seismic wave velocities show that the temperature variations in the deep mantle, that accompany the compositional layering, are on the high side.

Contents

1	Introduction	5
1.1	Introducing the model of compositionally layered mantle convection	5
1.2	Previous work	6
1.3	Mantle constraints	7
1.4	How may compositional layering have originated?	8
1.5	Problem definition	9
2	Model Description	10
2.1	Governing physical processes	10
2.2	The equation of state	11
2.3	A set of dimensionless equations	11
2.4	Numerical method	12
2.5	Composition-dependent density and heat production	13
2.6	Initial conditions for temperature, mass density and viscosity	14
2.7	Post-processing programs	14
2.8	Introduction to the six different models used	15
3	Dynamic Evolution of the Reference Model	16
3.1	Layered convection in the first 2.0 Gyr	16
3.2	Material flux across the phase transition: non-layered convection	17
3.3	Convectively induced topography and layer stability	17
3.4	The lifecycle of oceanic lithosphere	20
3.5	Relating the heat flux across the CMB to the Earth's magnetic field	21
3.6	Conclusions	23

4	Sensitivity to Variations in Thermal Conditions	24
4.1	The thermal blanketing effect of the deep mantle reservoir	24
4.2	Uniform radioactive heat production	27
4.3	The influence of thermal core coupling	27
4.4	Scaling the internal heating rate in the mantle	27
4.5	Conclusions	28
5	Predicting Seismic Wavespeed Variations	29
5.1	Calculating seismic wavespeed variations	29
5.2	Wavespeed variations in the reference model	30
5.3	Wavespeed variations for a gradual initial compositional gradient	32
5.4	Wavespeed variations in model D0	33
5.5	Conclusions	36
6	Discussion	37
6.1	Approximations in the theoretical framework	37
6.2	Numerical approximations	38
6.3	Discussion of the model results	38
7	Conclusion	40
8	Acknowledgements	42
A	Thermal Coupling of the Earth’s Mantle and Core	46
B	Calculation of a time-dependent buoyancy number and entrainment	47
B.1	Quantifying a time dependent buoyancy number	47
B.2	Quantifying the entrainment of deep mantle reservoir material	47
C	Calculation of Seismic Velocity Anomalies	48
C.1	Calculating temperature and compositional density perturbations	48
C.2	Dependence of velocity on temperature and composition	49
D	Modelling Density Variations in an Incompressible Flow Model Using a Penalty Function Approach	50

Glossary of terms

symbol	property	RFM value	dimension
A	surface area		m^2
B	buoyancy parameter		–
C	heat capacity		JK^{-1}
c_P	specific heat	1250	$Jkg^{-1}K^{-1}$
d_0	dim.less initial thickness deep mantle reservoir	0.2	–
d_{ph}	thickness phase transition	1×10^5	m
Di	dissipation number	0.46	–
f	heat capacity fraction mantle to core	0.8	–
g	gravitational accelaration	9.8	ms^2
h	mantle depth	2.9×10^6	m
H	heat production		Wkg^{-1}
k	thermal conductivity	5	$Wm^{-1}K^{-1}$
P	pressure		Pa
P_{ph}	reference pressure phase transition	2.4×10^{10}	Pa
p	prefactor viscosity	100	–
q	heat flow density		Wm^{-2}
Q	total heat flux		W
R	seismological parameter		–
R_0	internal heating number	21.80	–
Ra	thermal Rayleigh number	1.07×10^9	–
Rb	compositional Rayleigh number		–
t	time		s
T	temperature		K
T_{srfc}	surface temperature	273	K
T_{core}^0	initial core temperature	4273	K
T_{ph}	reference temperature phase transition	2073	K
ΔT	temperature scale value	4000	K
u	mantle flow velocity		ms^{-1}
V	volume		m^3
z	dimensionless depth		–

α	thermal expansivity		K^{-1}
α_0	surface value thermal expansivity	2×10^{-5}	K^{-1}
$\Delta\alpha$	th. exp. contrast across mantle ($\frac{\alpha_{CMB}}{\alpha_0}$)	0.2	–
η	dynamic viscosity		$Pa\cdot s$
η_0	reference viscosity	5×10^{20}	$Pa\cdot s$
$\Delta\eta_P$	viscosity contrast due to pressure	100	–
$\Delta\eta_T$	viscosity contrast due to temperature	20	–
γ	Clapeyron slope	-2.5×10^6	PaK^{-1}
Γ_c	composition function		–
Γ_{ph}	phase function		–
κ	thermal diffusivity	1.176×10^{-6}	m^2s^{-1}
ρ	mass density		kgm^{-3}
ρ_0	reference mass density	3400	kgm^{-3}
$\Delta\rho$	effective composite density perturbations		kgm^{-3}
$\frac{\delta\rho_c}{\rho_0}$	relative compositional density jump	0.015	–
$\frac{\delta\rho_{ph}}{\rho_0}$	relative density jump phase transition	0.1	–
$\tau_{1/2}$	half-life time of radioactive decay	2.5×10^9	yr

Table 1: Explanation of symbols. The values in the third column were used in the reference model RFM.

subscript	meaning
0	reference, scale or surface value
c	composition
core	core
CMB	core mantle boundary
dm	deep mantle
h	heating
int	interface
init	initial
man	mantle
mm	mid-mantle
ph	phase
sfrc	surface
T	temperature
up	upper mantle

Table 2: Explanation of subscripts.

Chapter 1

Introduction

The mantle is known to play a prominent role in the Earth's thermal, dynamic and chemical evolution. Also, the mantle directly influences processes observed in the crust, such as plate tectonics and intra-plate volcanism. In our quest to understand the behaviour of the mantle, a wide variety of models have been considered (see Tackley (2002) for an overview). In recent years, the model of compositionally layered mantle convection (e.g. Kellogg et al. (1999), Hansen and Yuen (2000), Tackley (2002)) has become increasingly popular due to indications from various fields of research. The purpose of the study presented in this report, is to investigate the dynamic feasibility of the proposed model of compositionally layered mantle convection.

1.1 Introducing the model of compositionally layered mantle convection

Compositionally layered mantle convection is illustrated in Figure 1.1 (from Kellogg et al. (1999)). In this case, the mantle contains two reservoirs, which are convectively isolated; they do not mix. Firstly, the upper and mid-mantle form a single reservoir, in which the convective flow is expressed in cold downwelling slabs of oceanic crust and hot upwelling mantle plumes. Separated from this, is the deep mantle reservoir, which overlies the D"-layer and is characterised by a balance between positive and negative buoyancy forces. A negative buoyancy force results from the excess compositional density, where the deep mantle is a few percent more dense than the overlying material. On the other hand, a positive buoyancy force is caused by the temperature difference between the two reservoirs, possibly promoted by an enlarged heat production rate in the deep mantle.

When the positive and negative buoyancy forces nearly balance, a situation may emerge where the deep mantle reservoir is stable, but shows substantial topography. This topography is induced by subducting slabs, that sweep the deep mantle layer into piles, extending up to several 100's of kilometers above the core. The stability of the reservoir is quantified by the buoyancy number B , which gives the ratio of the negative compositional to the positive thermal buoyancy, i.e. $B = \frac{\delta\rho_c}{\delta\rho_T} = \frac{1}{\alpha_0\Delta T} \frac{(\delta\rho)_c}{\rho_0}$. Values larger than one are associated with long-term stability.

1.3 Mantle constraints

Compositionally layered mantle convection is supported by indications from various fields of geophysical and geochemical research. The constraints formulated by these disciplines are discussed below.

1. Geochemistry: distinct mantle reservoirs

Surface basalts can be divided into two distinct groups. Firstly, Mid-Oceanic Ridge Basalt (MORB) forms at spreading ridges, where diverging plates cause mantle material to rise. During this uplift, partial melting takes place and incompatible elements, including radiogenic isotopes such as Thorium and Uranium, rise to the Earth's surface to form the basaltic oceanic crust. As a consequence, the underlying melt residu (the Harzburgite layer) is depleted in incompatible elements. MORB is of relatively homogeneous composition around the world, indicating that the MORB-source region is well-mixed. Secondly, oceanic island basalts (OIB's) are found in hot-spot areas, where the melt products of hot mantle plumes are believed to form crustal material. The isotopical signature of OIB is more heterogeneous as compared to MORB.

The chemical differences between the two types of surface basalts indicate that they sample chemically distinct, convectively isolated mantle reservoirs (e.g. Hofmann (1997)). More precisely, geochemical studies of isotope abundances, such as He, Ar, K, U and Th, favour the existence of one or more long lived, isolated mantle reservoirs (Turcotte et al. (2001) and Albarede (2002)). Such reservoirs would have been isolated from chemical differentiation by partial melting and outgassing. They must have been well-preserved during a long period of time in the Earth's evolution and are therefore often referred to as 'primitive'.

2. Seismic tomography: material flux across the phase transition

The geochemical arguments above have lead to the model of convection, strictly layered at the 660-km phase transition, in the 1960's. This conventional model was rejected when tomographic evidence accumulated in the 1990's (e.g. Van der Hilst and Engdahl (1997)), indicating that some of the subducting plates are able to move through the phase transition. Other subducting lithosphere seems to be restricted to the upper mantle.

3. Seismology: chemical component in the lowermost mantle

Seismological studies (Masters and Laske (2000)), indicate that in the lowermost mantle the radial variation in P-wave speed is up to 1% and that in S-wavespeed about twice as large. Two large areas of low seismic velocity are situated beneath the Pacific ocean and beneath Africa. These are commonly interpreted as hot upwelling areas.

However, Van der Hilst and Karason (1999) explain that several lines of geophysical evidence imply that these heterogeneities are hard to explain on a purely thermal basis. They argue that compositional stratification in the lower 1200 km of the mantle could explain the observations. In this light the seismological parameter R plays an important role. R gives the ratio between S- and P-wavespeed variations ($R = \frac{\delta \ln v_s}{\delta \ln v_p}$). Values for R larger than 2.5 are believed to originate, in addition to thermal effects, from chemical anomalies. In the lowermost mantle values around 2.5 are observed (see Figure 5.6 from Masters and Laske (2000)), although the resolution at these large depths makes a conclusive interpretation very hard.

4. Heat budget calculations: extra heat source

The present-day surface heat-flux of 44 TW must be explained by a combination of radioactive heat production and cooling of the Earth. If the mantle solely contains MORB-source material, which is depleted in heat producing elements, then the volume integrated heat production falls significantly below the total present-day surface heat flux. As a consequence, the Earth would cool very rapidly. Parameterised convection models studying the thermal history (e.g. Honda (1995) and Richter (1985)) show that in a monotonic secular cooling scenario, this requires unrealistically large temperatures during the Archaean. To account for more realistic cooling regimes, one or more extra heat sources in the mantle are needed. A convectively isolated dense layer in the deep mantle could provide the location of such a heat source.

5. Seismology: unsuccessful search for seismic reflections

In contrast to the indications above, which were all favouring compositionally layered convection, there is a strong argument against it. Despite recent studies (Vidale and Schubert (2001) and Castle and Van der Hilst (2000)), seismic reflections from a chemical interface between two reservoirs have not been found. A possible explanation, without having to reject the compositionally layered model, is that the interface is hard to detect. This could be caused by its sloping surface, or by a gradual, rather than sharp, chemical boundary layer.

1.4 How may compositional layering have originated?

Apart from being dynamically stable and satisfying the mantle constraints, the origin of the deep mantle must be explained. Three candidate mechanisms for the formation of the layering are given below.

1. Development during the early differentiation of the Earth

In the hot early Earth a (partially) liquid magma ocean was likely to be present. Chemical differentiation, due to fractional crystallisation of a magma ocean, could have lead to a layered early Earth. The characteristics of such a magma ocean depend on the conditions during the Earth's formation (Abe (1996)), which are highly uncertain.

2. Formation and recycling of a mafic crust

In a high temperature-pressure environment, crustal basalt transforms into high-density eclogite, which is enriched in heat producing elements. At present, eclogite is formed in subducting slabs. If the eclogite segregates from the buoyant Harzburgite, it may still be added to the deep layer today (Christensen and Hofmann (1994) and Irifune and Ringwood (1993)). In the Archaean, a large eclogite production rate may have been caused by the high pressure at the base of a thick oceanic crust (Vlaar et al. (1994)). An important fraction of this eclogite may have sunk towards the lower parts of the mantle and accumulated into a chemically distinct layer, which is enriched in radioactive elements.

3. Core-mantle interactions

Processes associated with chemical interactions between the core and the mantle may have affected the chemical state of the lowermost mantle (Loper and Lay (1995), Jeanloz and Lay (1993)).

1.5 Problem definition

Before a conclusive answer can be given to which model gives a proper description of the Earth's mantle, the constraints from the various fields of research need to be established more precisely. Until then, the model of compositionally layered mantle convection remains speculative. In spite of this remaining uncertainty, the model is capable of satisfying recent geophysical and geochemical constraints in which other models fail. The study presented here, examines compositionally layered mantle convection numerically. New aspects in this light are the incorporation of a phase transition and a thermal coupling model with the core. The study concentrates on the following three research questions.

1. Is compositionally layered mantle convection stable in a cooling mantle over a period of time comparable to the age of the Earth, i.e. 4.5 Gyr¹?
2. To what extent do the chosen input and output parameter values relate to values for the real Earth?
3. How sensitive is the model to variations in the model set-up? In particular the effects of compositional layering are examined on a) the thermal behaviour of the mantle and b) the seismic signature.

¹Although previous numerical studies have answered this question affirmative (see also Section 1.2), this has not been shown with the incorporation of a phase transition and thermal coupling with the core.

Chapter 2

Model Description

2.1 Governing physical processes

The numerical modelling experiments presented here are based on a thermo-chemical convection model. A set of four coupled partial differential equations (equations 2.1 to 2.4) describe the governing physical processes mathematically, i.e. transport of mass, momentum, heat and chemical composition. We use the cartesian coordinate system, where z points downward. Symbols and values used are explained in Table 1. A detailed derivation is given in Van den Berg and Vlaar (2001).

The velocity field is divergence-free and the mass balance equation is given by

$$\nabla \cdot \vec{u} = 0 \tag{2.1}$$

In the Stokes equation, an infinite Prandtl number is assumed. Viscous fluid flow depends on pressure and gravity variations as follows.

$$-\nabla \Delta P + \eta(T, P) \nabla^2 \vec{u} + \Delta \rho \vec{g} = \vec{0} \tag{2.2}$$

The energy equation (equation 2.3) describes heat transport and includes advection of heat, adiabatic (de-) compression, heat diffusion and frictional and radioactive heat production. Latent heat and melting are being neglected.

$$\rho_0 c_P \frac{dT}{dt} - \alpha(z) T \frac{dP}{dt} - \nabla \cdot (k \nabla T) - \tau : \nabla \vec{u} - \rho_0 H(t) = 0 \tag{2.3}$$

In the advection equation for composition (equation 2.4), diffusion of material is excluded. Hence, compositional heterogeneities in the mantle are able to mix by means of material flow only.

$$\frac{\partial \Gamma_c}{\partial t} + (\vec{u} \cdot \nabla) \Gamma_c = 0 \tag{2.4}$$

2.2 The equation of state

The mass density ρ depends on temperature variations, on the phase and on compositional variations. Mass density is given by the equation of state:

$$\rho(T, P, \Gamma_c) = \rho_0 + \Delta\rho = \rho_0[1 - \alpha(z)(T - T_{srfc}) + \Gamma_{ph}(T, P)\frac{\delta\rho_{ph}}{\rho_0} + \Gamma_c\frac{\delta\rho_c}{\rho_0}] \quad (2.5)$$

The depth-dependent thermal expansivity in equation 2.5 is parameterised by

$$\alpha(z) = \alpha_0 \frac{\Delta\alpha}{((\Delta\alpha^{1/3} - 1)(1 - z) + 1)^3} \quad (2.6)$$

which states that $\alpha(z)$ decreases from α_0 at the top surface ($z = 0$) to $\alpha_0\Delta\alpha$ at the bottom of the convecting layer ($z = 1$). Figure 2.2c shows the depth-dependent behaviour of the thermal expansivity.

An endothermic phase transition with a negative Clapeyron slope $\gamma = \frac{dP}{dT}$, and a relative density increase $\frac{\delta\rho_{ph}}{\rho_0}$, represents the 660-km phase transition, which divides the upper from the lower mantle. The phase transition is located at a depth z_{ph} . This depth is defined as the location where the geotherm crosses the Clapeyron slope, which is fixed at a reference temperature T_{ph} and pressure P_{ph} . The T-,P-dependence of the location of the phase transition z_{ph} gives it a non-steady character. The parameterisation of the phase function Γ_{ph} , varies from zero to one over a depth range d_{ph} as

$$\Gamma_{ph}(T, P) = \frac{1}{2}[1 + \sin(\pi\frac{z - z_{ph}(T, P)}{d_{ph}})] \quad (2.7)$$

quantity	symbol	expression	value STD
thermal Rayleigh number	Ra	$\frac{\rho_0\alpha_0g\Delta Th^3}{\eta_0\kappa}$	1.07×10^9
compositional Rayleigh number	Rb_c	$\frac{\delta\rho_cgh^3}{\eta_0\kappa}$	1.34×10^{10}
phase Rayleigh number	Rb_{ph}	$\frac{\delta\rho_{ph}gh^3}{\eta_0\kappa}$	8.9×10^{10}
surface buoyancy number	B_0	$\frac{Rb_c}{Ra} = \frac{1}{\alpha_0\Delta T} \frac{\delta\rho_c}{\rho_0}$	0.19
dissipation number	Di	$\frac{\alpha_0gh}{c_P}$	0.45
internal heating number	R_0	$\frac{H_0h^2}{c_P\kappa\Delta T}$	21.80

Table 2.1: Dimensionless numbers, their expressions and values in the reference model.

2.3 A set of dimensionless equations

Equations 2.1 to 2.4 were combined with the equation of state (equation 2.5) and scaled to their dimensionless forms to make the model results easy comparable with other studies. The following

scaling operations were used.

$$\begin{aligned} \vec{x} &= \vec{x}'h, & t &= t'h^2/\kappa, & T &= \Delta T(T' + \frac{T_{srfc}}{\Delta T}), & \Delta P &= \Delta P' \frac{\eta_0 \kappa}{h^2}, \\ \tau &= \tau' \frac{\eta_0 \kappa}{h^2}, & \vec{u} &= \vec{u}' \frac{\kappa}{h}, & \eta &= \eta' \eta_0, & H &= H' H_0, & \alpha &= \alpha' \alpha_0 \end{aligned} \quad (2.8)$$

Finally, the following set of dimensionless equations was obtained, describing an incompressible, extended-Boussinesq fluid at infinite Prandtl number. The accents, introduced in equation 2.8, were dropped.

$$\nabla \cdot \vec{u} = 0 \quad \text{mass conservation equation} \quad (2.9)$$

$$-\nabla \Delta P + \nabla^2 \vec{u} + (RaT - Rb_{ph}\Gamma_{ph} - Rb_c\Gamma_c)\hat{z} = \vec{0} \quad \text{equation of motion} \quad (2.10)$$

$$\begin{aligned} \frac{dT}{dt} - Di\alpha(z)u_z(T + T_0) \\ -\eta(T, P)\nabla^2 T - \frac{Di}{Ra}\tau\nabla\vec{u} - R_0H(t) = 0 \end{aligned} \quad \text{energy equation} \quad (2.11)$$

$$\frac{\partial\Gamma}{\partial t} + (\vec{u} \cdot \nabla)\Gamma_c = 0 \quad \text{comp. transport equation} \quad (2.12)$$

In this set of equations, the dimensionless numbers play an important role; they control the behaviour of the convection. They are listed in Table 2.1 together with their values for the reference model.

2.4 Numerical method

To solve the mathematical expressions, they were first translated to their discretised forms using finite elements methods (see Van den Berg (2000)). Equations 2.1 to 2.3 were solved using a Eulerian convection code, developed at the Department of Theoretical Geophysics of the University of Utrecht. The code is based on the SEPRAN finite element code (Segal and Praagman (2000)). Time integration of the coupled set of equations was done using a predictor-corrector scheme (see Van den Berg et al. (1993)).

The equation for composition transport (equation 2.4) is solved using a Lagrangian tracer particle method. Here, the tracer particles are carried by the convective flow of material (see Van Hunen (2001) and Van Thienen et al. (ress)).

Numerical calculations were performed on a 2-D cartesian box with aspect ratio 2.5 (see Figure 2.1. The numerical mesh contains 100 elements in the x-direction and 55 in the z-direction, with 45 elements between $z=.1$ and $z=1.$ and 10 elements between $z=0.$ and $z=.1.$ Thus, a two times higher resolution was imposed near the surface, where large temperature and viscosity variations were expected. In total, 11,000 finite elements were used and 250,000 tracer particles, which were initially placed at uniformly random locations.

All material boundaries are free-slip and impermeable. For temperature, natural boundary conditions were assigned to the vertical sides of the model, corresponding to lateral symmetry conditions.

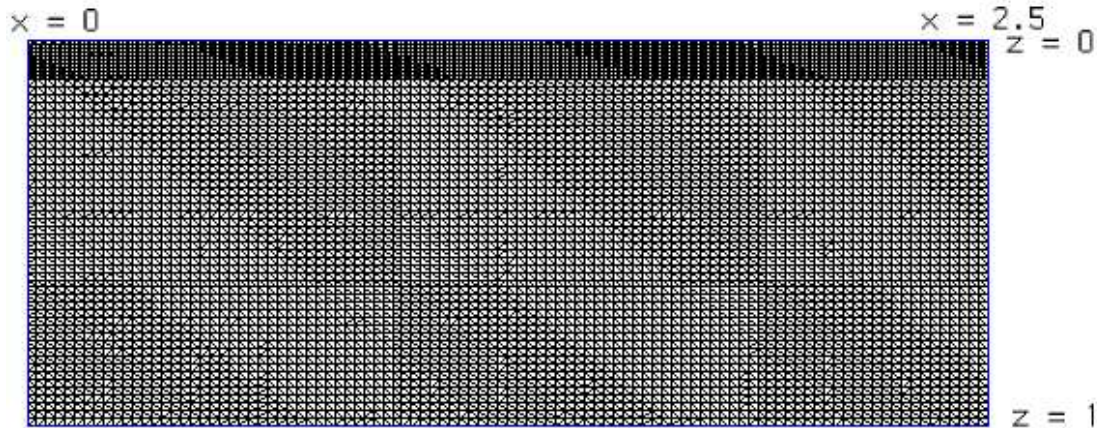


Figure 2.1: Geometry of the numerical mesh. The resolution of the finite elements is doubled near the top surface.

	temperature	flow velocity
top	$T = T_{srfc}$	$u_z = 0, \frac{\partial u}{\partial z} = 0$
sides	$\frac{\partial T}{\partial x} = 0$	$u_z = 0, \frac{\partial u}{\partial z} = 0$
bottom	core coupling	$u_z = 0, \frac{\partial u}{\partial z} = 0$

Table 2.2: Boundary conditions in the reference model RFM.

The top was kept at a constant temperature of $0^\circ C$. For the bottom boundary, conductive heat exchange between the mantle and core was simulated. The thermal coupling model used, is based on an isothermal heat reservoir representation for the core (see Appendix A for a description).

2.5 Composition-dependent density and heat production

For the initial compositional conditions, all tracers above the layer depth d_0 ($z = 0.8$) were given the composition value zero, and tracers below d_0 were given the composition value one, representing the deep mantle reservoir. Values for the radioactive heat production and density were then assigned to each tracer individually, depending on their compositional value.

Equation 2.5 shows that mass density depends on temperature, phase and composition. The relative compositional density perturbation is equal to $\frac{\delta \rho_c}{\rho_0}$, where the largest values are for the deep mantle reservoir, with the compositional value of one.

The radioactive heat productivity also depends on composition. It decays with time and was parameterised as

$$H(t, \Gamma_c) = H_0 [1 + \Gamma_c] e^{-\frac{\ln(2)}{\tau_{1/2}} t} \quad (2.13)$$

where $\tau_{1/2}$ represents the half-life time of the radioactive elements. In the reference model, the heat productivity was chosen twice that of the overlying mantle. First, the values were chosen such that the mantle as a whole has a chondritic heat production rate. After 4.5 Gyr of radioactive decay, the volume averaged rate of heat production is $5.0 \times 10^{-12} \text{Wkg}^{-1}$. To these heat productivity values, a multiplication of 0.614 was then applied, to correct for the overestimation of the volume-to-surface ratio of the cartesian geometry of the model domain.

2.6 Initial conditions for temperature, mass density and viscosity

The initial temperature field was chosen as a uniformly hot mantle, which has been cooled for 60 Myr from the top boundary, which is kept at a fixed temperature of zero degrees centigrade. Figure 2.2a shows the resulting temperature profile. This temperature field was chosen to avoid large temperature variations near the upper boundary, which are numerically not desirable. Added to this temperature field, was a positive temperature perturbation in the upper right corner, and a negative perturbation in the upper left corner. These two perturbations serve to induce the convective circulation and to avoid any artificial stability.

The dependence of density on phase and composition was explained in Section 2.5. Figure 2.2d shows the initial density profile, which was calculated from the equation of state (equation 2.5). The two density jumps represent the phase transition around 660-km depth and compositional density variations, initially at 2320 km depth. Except for these localised jumps, the density gradually changes throughout the mantle. These changes are controlled by a strong temperature increase in the upper mantle and the variation of thermal expansivity throughout the mantle.

The viscosity is dependent on temperature and depth and is given by

$$\eta(T, z) = \eta_0 p e^{-\ln \Delta(\eta_T)T + \ln \Delta(\eta_P)z} \quad (2.14)$$

Figure 2.2b shows the viscosity profile for the initial temperature distribution. A high viscosity zone at the cold, fixed temperature surface, representing the Earth's lithosphere, is automatically generated. It overlies a low viscosity zone, simulating the asthenosphere. At larger depths, the depth-dependence of the rheology leads to an increase in viscosity.

2.7 Post-processing programs

In order to improve the analyses of the results, two FORTRAN post-processing programs were written. The first one serves to quantify a) the amount of entrainment of deep mantle material in the depleted mantle and b) a time dependent buoyancy parameter. A detailed description of this program can be found in Appendix B. The second program predicts the seismic P- and S-wave velocity perturbations, from the temperature and compositional fields. A description of this program is given in Appendix C. The predicted velocity variations will be compared with seismological data in Chapter 5.

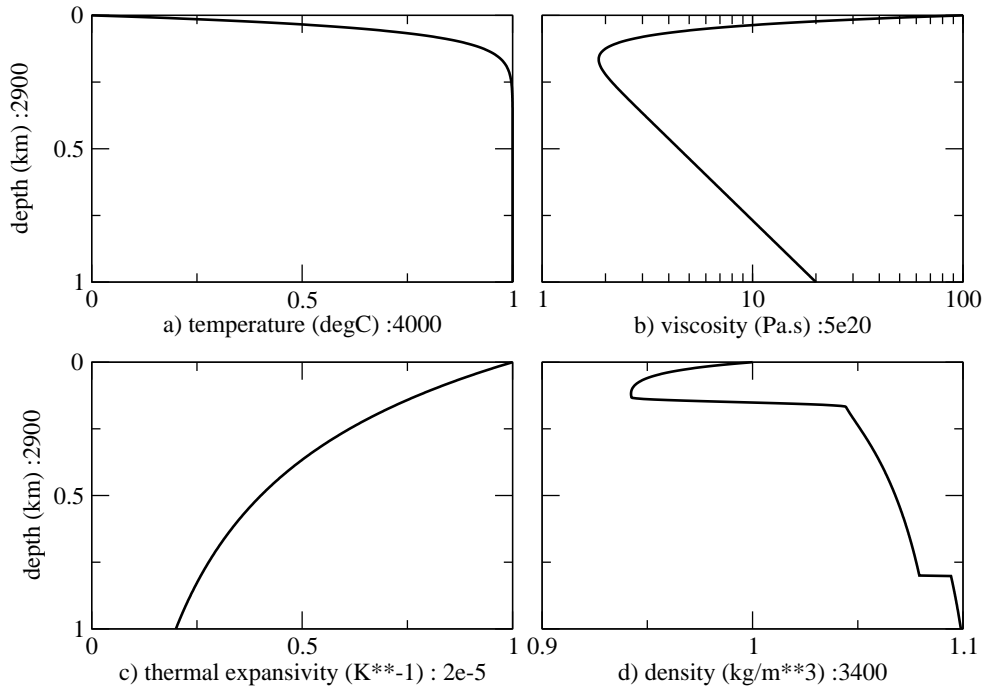


Figure 2.2: Initial conditions for a) temperature, b) viscosity, c) thermal expansivity and d) density.

2.8 Introduction to the six different models used

The preceding paragraphs described the design of the reference model RFM. The results of this model are given in Chapter 3. In addition to the reference model, five models were generated to test the sensitivity of the reference model to certain changes in the model. These test models will be discussed in Chapter 4 and 5. Table 2.3 gives the input values that are different from the reference model.

symbol	quantity	RFM	D0	UNIF	TC	SCLD	LIN	dimension
H_{0um+mm}	up.+mid-mantle heat pr.	15.48	18.57	18.57	15.48	25.21	15.48	$10^{-12}Wkg^{-1}$
H_{0dm}	deep mantle heat prod.	30.95	–	18.57	30.95	50.41	30.95	$10^{-12}Wkg^{-1}$
d_0	diml. thickness deep layer	0.2	0	0.2	0.2	0.2	*	–
f	C_{man}/C_{core}	0.8	0.8	0.8	∞	0.8	0.8	–

Table 2.3: Parameters values for all models. (*): in model LIN the composition increases linearly from 0 at $z = .6$ to 1 at $z = 1$. Here, the excess composition, integrated over the mantle, is equal to that in the reference model.

Chapter 3

Dynamic Evolution of the Reference Model

The characteristics of the reference model, *RFM*, were described in Chapter 2 and the input parameter values used, are listed in Tables 1 and 2.3. The excess compositional density in the deep mantle reservoir is 1.5%, giving a value of 0.19 for the surface buoyancy ratio B_0 . The surface Rayleigh number Ra_0 is 1.07×10^8 , the internal heating number R_0 is 21.80 and the dissipation number Di is 0.46 (see also Table 2.1). Figure 3.1 shows time snapshots of composition, temperature and viscosity fields. Together with the graphs in Figure 3.2, the model evolution will be described chronologically.

3.1 Layered convection in the first 2.0 Gyr

During the first 2.0 Gyr, convection is strictly layered at both the phase transition and the compositional interface, as indicated by the streamlines in Figure 3.1b and the vertical flow velocity in Figure 3.2b. Thus, the mantle is divided into three, convectively isolated reservoirs: the upper, mid- and deep mantle.

In this early period, the upper mantle loses a large amount of heat to the cold surface, as is indicated by the large surface heat flux (Figure 3.2g, top curve). Consequently, the upper mantle cools relatively fast ($\sim 1700^\circ C$ in the first 893 Myr alone, see Figure 3.2a).

In the mid-mantle, temperatures slightly increase (Figure 3.2a). However, the reservoirs by which it is enclosed, cool down (upper mantle) and heat up (deep mantle) significantly. As a result of this growing temperature difference across the mid-mantle, the vigour of convection increases with time. Still, at these early times, the convective vigour in the mid-mantle is too small (Figure 3.2b,e) to cause significant topography (figure 3.1a), and the deep mantle reservoir remains as a nearly flat layer on top of the core.

The deep mantle reservoir is thermally insulated between the mid-mantle and the core. Because of its large radioactive heat production (twice that of the rest of the mantle), the temperature in the deep mantle starts to rise. Figure 3.2d (red curve) shows that, during the first 2.0 Gyr, temperatures in the deep mantle increase up to $4600^\circ C$. This value is larger than the core temperature (top black curve in Figure 3.2d) and therefore heat flows from the deep mantle into the core (figure 3.2g,

bottom curve). As a consequence, the core temperature rises with approximately $100^\circ C$ after 2 Gyr model time (figure 3.2d, top black curve).

3.2 Material flux across the phase transition: non-layered convection

After a model time of 2.0 Gyr the layered style of convection breaks down. The dynamic regime and the thermal evolution of the model changes drastically after this transition, as now will be described.

As the upper mantle cools down, the subducting slabs grow larger and stronger. This enables the strongest slabs to break through the phase transition and penetrate the lower mantle. These so-called 'mantle avalanches' first occur at 2.0 Gyr and continue until the model stops after 4.5 Gyr. The phase transition now acts as a filter; while small slabs are restricted to the upper mantle, larger ones penetrate the lower mantle. Thus, the observed convection regime is in between the two end-members of layered and whole mantle convection. This convection regime of occasional material flux across the phase transition will be referred to as 'non-layered convection'. Steinbach et al. (1993) already noticed the breakdown of layered convection in a cooling mantle, thereby showing the importance of a phase transition in evolutionary mantle models.

Mantle avalanches drive the convection in the upper and mid-mantle, as is indicated by the large flow velocities (see Figure 3.1b at $t = 3572.8$ Myr and the peaks in the root-mean-squared velocity in Figure 3.2e). The increased vigour of convection is accompanied by a more pronounced cooling rate and results in an increase in viscosity (see Figure 3.2a,c,d). Another effect of the increased vigour of convection is the more pronounced surface heat flux (Figure 3.2g, top curve). After 4.5 Gyr, a value of 150 mWm^{-2} is reached, which is approximately twice the present-day value.

Figure 3.1b,c shows that in the non-layered style of convection, large quantities of upper mantle material are replaced, suggesting large scale resurfacing events. Larson (1991) discusses the geological indications for resurfacing events as recently as the Cretaceous (~ 100 Ma).

3.3 Convectively induced topography and layer stability

In the layered convection regime, the deep mantle reservoir remained as a continuous, nearly flat layer on top of the CMB. The situation changes after the transition to the non-layered convection regime. Then, the strong slabs that reach the lower mantle sweep the deep mantle reservoir into isolated mounts of material (Figure 3.1a, last three snapshots), although the continuity of the layer recovers at quiet periods (not shown).

The amount of topography induced on the chemical interface depends on the stability of the deep layer. This stability is model-dependent; it increases with a larger chemical buoyancy or a smaller thermal buoyancy. Large chemical buoyancy is promoted by a large compositional excess density.

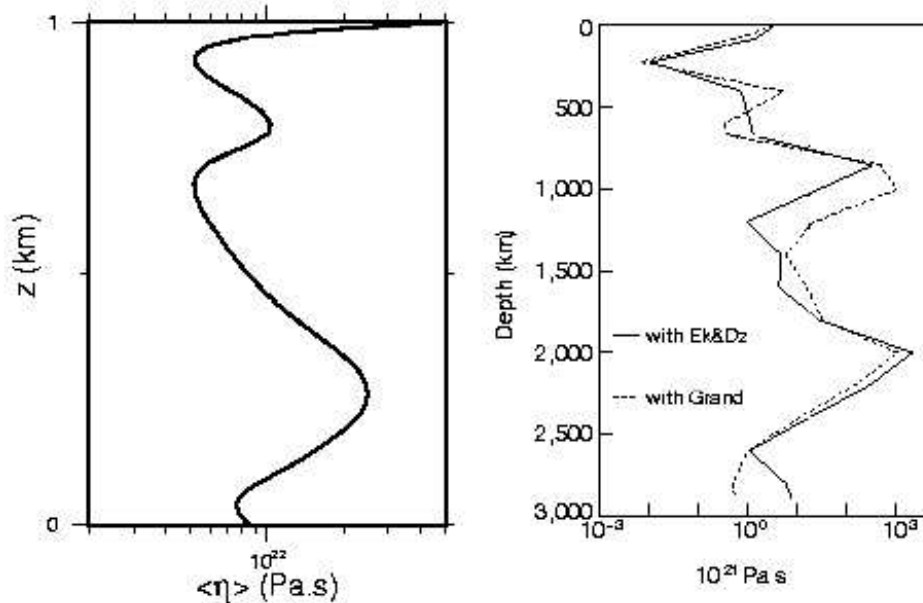


Figure 3.4: left: Viscosity profile for the reference model after 4.5 Gyr model time. right: Viscosity profiles from Forte and Mitrovica (2001) based on the seismic models of Grand et al. (1997) (dashed line) and Ekstrom and Dziewonski (1998)(solid line).

3.5 Relating the heat flux across the CMB to the Earth’s magnetic field

The mean heat flow density across the CMB (Figure 3.2g, bottom curve) shows that the core gains heat from the mantle in the period of layered convection (<2.0 Gyr) and therefore heats up (Figure 3.2d, top black curve). It is only after the transition to non-layered convection, that this heat flow into the core stops, when contact between the cold descending slabs and the hot core becomes more frequent. While in the reference model the total heat flux remains close to zero, other models investigated (see model D0 in Section 4.1 and model LIN in Chapter 5) show that a larger, more realistic total heat flux of ~ 5 TW out of the core (Buffett (2000)) is not unlikely.

A heat flow out of the core is necessary for driving the geodynamo, which generates the Earth’s magnetic field. From paleomagnetic studies it is inferred that the magnetic field has existed in its current form for at least 2.7 Gyr. An overview of paleo-intensity studies from Sumita et al. (2001) is given in Figure 3.5. The jump in intensity at ~ 2.7 Ga roughly correlates with the predicted jump in heat flux across the CMB at 2.0 Gyr (~ 3.5 Ga). Thus, the numerical results are not in contradiction with the paleomagnetic data. However, Archaean rock samples with a reliable imprint of the Earth’s magnetic field are in short supply and are often of poor quality. Therefore, the data in Figure 3.5 is insufficient as a constraint on the core heat flux. A more funded comparison may become possible when more reliable data from paleo-intensity studies becomes available.

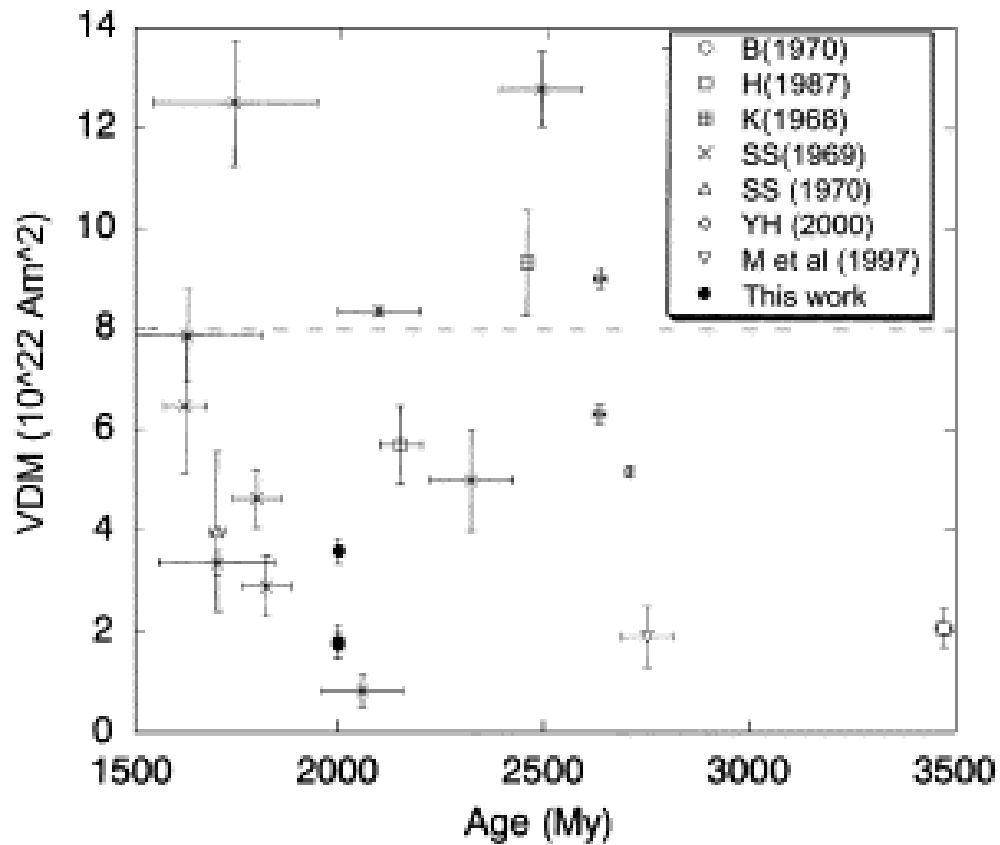


Figure 3.5: Overview of paleointensity studies (from Sumita et al. (2001)), showing the strength of the Earth's magnetic field during Archaean and Proterozoic times. Plotted on the vertical axis is the virtual dipole moment (VDM). The present-day value ($\sim 8 \times 10^{22} \text{ Am}^2$) is indicated by the dashed line.

3.6 Conclusions

The main conclusions from the results of the reference model are listed below.

- Stable compositional mantle layering with substantial topography, over a model time of 4.5 Gyr, is produced by choosing a compositional excess density of around 1.5% ($B_0 = 0.19$) for the deep mantle reservoir. The stability limit is estimated at $\sim 1\%$ extra compositional density ($B_0 = 0.13$)
- Mantle evolution is characterised by a transition from layered to non-layered convection, at 2.0 Gyr model time. The transition occurs when the subducting slabs in the cooling upper mantle grow large and strong enough to cross the endothermic phase transition.
- After 2.0 Gyr, the phase transition acts as a filter to subducting slabs; it restricts weak slabs to the upper mantle, while the stronger slabs penetrate the lower mantle and cause topography on the deep mantle reservoir.
- After 4.5 Gyr model time, the surface heat flux, mantle temperatures and flow velocities show a reasonable resemblance with present-day mantle values, although mantle temperatures and the surface heat flux are on the high side. A large viscosity zone around 2200 km depth, after a model time of 4.5 Gyr, is in agreement with the study of Forte and Mitrovica (2001).
- The core heat flux, predicted in the numerical results, does not contradict paleomagnetic data, although this data is insufficient as an important constraint on the core heat flux. Negligible core cooling seems unrealistic in view of the necessity of core cooling for the geodynamo and crystallisation of the inner core.

Chapter 4

Sensitivity to Variations in Thermal Conditions

In order to examine the behaviour of compositionally layered mantle convection in more detail, four sensitivity tests have been performed. These tests serve to estimate the response of the reference model to a) the presence of the deep layer, b) its increased radioactive heat production, c) the thermal coupling with the core and d) the geometric scaling of the heat production in a 2-D, cartesian model.

4.1 The thermal blanketing effect of the deep mantle reservoir

In Section 3.5, the importance of the blanketing effect of the deep layer on the core, and its implications on the Earth's magnetic field, was mentioned. To examine this blanketing effect, the deep layer was removed in model D0. The volume averaged heat production is equal to that of the reference model, which resembles the chondritic value and decays to a value of $5 \times 10^{-12} \text{W kg}^{-1}$ after 4.5 Gyr model time (see Table 2.3).

The results of model RFM and D0 are compared in Figures 4.1a,b and the black and blue curves in Figure 4.2. During the period of layered convection, the presence of the deep layer on the dynamic model behaviour is small. It is only after the transition to non-layered convection, that the two models start to deviate from each other. Then, in the absence of a compositional layering, the cold subducting slabs reach the hot core without the hindrance of a dense reservoir. As a result, the heat flux out of the core is much more pronounced after 1.6 Gyr model time (Figure 4.2c). Consequently, the core cools faster, as is indicated in Figure 4.2b.

The above illustrates that the thermal blanketing effect of the deep layer is not primarily caused by the enlarged heat production of the deep layer, but rather by its ability to limit the contact between the hot core and the cold subducting slabs.

4.2 Uniform radioactive heat production

In the reference model, the heat production rate in the deep mantle reservoir was twice of that in the mid- and upper mantle (see Table 2.3). The impact of this increased heat production on the evolution was examined using the test model UNIF. In this model, the heat production is distributed uniformly over the mantle. Similar to the previous test model, the volume averaged heat production of the whole mantle is equal to that of the reference model, which is the chondritic value.

Figure 4.1 (black and purple curves on the right) shows that the smaller radioactivity in model UNIF leads to slightly lower temperatures in the lowermost mantle. Therefore, the heat flow into the core is also smaller than in the reference model (Figure 4.2c, black and purple curves). Similarly, slightly larger temperatures appear in the upper and mid-mantle. However, these temperature effects are small and as a result, the final snapshots of the models RFM and UNIF (Figure 4.1a,c) indicate that the dynamic behaviour of the two models is similar up to a large degree.

In Section 1.1 was explained that the stability of compositional layering depends on the temperature difference between the layers. In turn, this temperature difference is dependent on a) a different cooling rate of the two separate layers and b) a different radioactive heat productivity inside the two layers. Comparing model RFM and model UNIF gives insight in which of these effects is dominant. They show that the effect of the heat productivity distribution on the temperature difference between the layers is small. It thus follows that the different rate of cooling is the most important process in creating temperature differences between the two reservoirs and hence thermal instability of the compositional layering.

4.3 The influence of thermal core coupling

In model TC the thermal coupling with the core on the bottom boundary is replaced by a zero heat flux boundary condition. The influence of this thermal boundary condition on the dynamic evolution of the model is small (see Figure 4.1a,d and Figure 4.2, green curves). However, the absence of heat flow from the core leads to faster mantle cooling, resulting in about 300°C lower CMB temperatures after 4.5 Gyr (Figure 4.2a, black and green curves), or alternatively a substantial timeshift of ~ 700 Myr in the secular cooling of the mantle.

Without the thermal core coupling model, mantle temperatures near the CMB are preserved more easily than in the reference model. Thus, the heat producing layer stays hot, and the cold downwellings reaching the CMB stay cold and rigid for a longer period of time. In other words; when heat coupling with the core is included, subducted slabs gain heat from the core more quickly. This increases their mobility, leading to smaller residence times of slabs in the deep mantle.

4.4 Scaling the internal heating rate in the mantle

In a 2-D, cartesian model, the volume-to-surface ratio of the mantle is overestimated with a factor 1.629. Consequently, the volume integrated heat production is exaggerated with the same amount. Therefore, in all of the previous models, the heat production rate was scaled with a factor $\frac{1}{1.629} =$

0.614. To investigate the impact of this volume-to-surface correction, a separate model run was performed without applying this scaling factor.

Figures 4.1 and 4.2 show the results of model SCLD, which again are to be compared with the reference model. As was expected, the enlarged radioactivity leads to higher mantle temperatures, lower viscosities, larger velocities, a lower cooling rate and a larger surface heat flux. Qualitatively, the dynamic behaviour of the two models is not very different. However, if a quantitative interpretation is desired, the exaggeration of the radioactivity in 2-D, cartesian models must not be neglected.

4.5 Conclusions

The main conclusions from the four sensitivity tests that were presented in this chapter are the following five.

- The deep layer thermally blankets the core, not only by means of its enlarged heat production, but even more by its ability to limit the contact between the hot core and cold convective downwellings by its physical presence.
- The thermal instability of the deep mantle slightly increases with its heat productivity. Much more important in creating thermal instability, however, is the cooling rate of the mid-mantle.
- Incorporating a thermal coupling between the mantle and core results in a delay in secular cooling and leads to a faster heating of cold slabs that have reached the CMB. It thereby increases their mobility and decreases their residence time in the deep mantle.
- When using 2-D, cartesian models, the volume of the mantle is overestimated by a factor 1.6. Scaling the radioactivity is important when models are to be interpreted quantitatively.
- Overall, the four sensitivity tests show that the general characteristics of the reference model are robust for the parameter space examined. In all tests, the transition from layered to non-layered convection around 2 Gyr was observed and the deep mantle reservoir remained stable for a model time of 4.5 Gyr.

Chapter 5

Predicting Seismic Wavespeed Variations

5.1 Calculating seismic wavespeed variations

In order to relate the modelling results with recent interpretations of seismological observations in the mantle, seismic wave velocities were computed, based on a linearisation of the temperature and compositional dependence of the seismic wave velocities. The method is explained in Appendix C. In the transformation from temperature and compositional variations to seismic velocity variations, the derivatives of seismic wave velocities to temperature, $\frac{\partial \ln v}{\partial T}$, and composition, $\frac{\partial \ln v}{\partial X}$, are needed. Unfortunately, these derivatives are poorly constrained, especially for composition. Ongoing research in the field of mineral physics might improve the results in the near future, however. Seismic derivative values for the lowermost mantle, used in this work, were deduced from the calculations of Trampert et al. (2001) and are listed in Table 5.1.

The compositional density ρ_c has to be linked to the volumetric proportion of the element (X), which causes this compositional density. Since $\frac{\partial \ln \rho}{\partial X}$ differs between various chemical components, the chemical signature of the deep mantle has to be known. Unfortunately, this is not the case; we do not know what chemical elements causes the extra density in the lower mantle. In absence of better information, the value for iron was chosen ($\frac{\partial \ln \rho}{\partial X_{Fe}}$), which is close to 0.2.

	$\frac{\partial}{\partial T}$	$\frac{\partial}{\partial X}$
$\partial \ln v_p$	-2.0×10^{-5}	0.05
$\partial \ln v_s$	-3.0×10^{-5}	-0.1
$\partial \ln \rho$	-	0.2

Table 5.1: Seismic temperature and compositional derivatives for the lower mantle. The values are derived from the results in Trampert et al. (2001).

Hilst (2000) show no signs of a sharp transitions. Therefore, alternative models including a gradual compositional gradient have recently become popular (e.g. Hansen and Yuen (2000) and Albarede and Van der Hilst (2002)). In search for alternatives for a sharp chemical interface, model LIN, with an initial compositional gradient was examined. The model parameters are in Table 2.3 and snapshots for composition, temperature, streamfunction and viscosity are in Figure 5.4. The model set-up is comparable to the work of Hansen and Yuen (2000).

Figure 5.4 shows snapshots for the results of model LIN. After 4.5 Gyr, the initial compositional gradient has transformed into two convectively isolated layers. Compositionally, the deep mantle reservoir becomes more homogeneous with time, although some heterogeneities within the layer exist after 4.5 Gyr. The mean compositional value of the layer is lower than in the reference model (see Figure 5.2a), which also means a smaller negative buoyancy force. This explains the lower stability of the deep mantle reservoir in model LIN. The entrainment outside the deep mantle reservoir is large, causing a more heterogeneous and enriched mantle outside the deep mantle. The interface between the layers is less sharp as in the reference model. This might explain the failure in finding seismic reflections on the interface. However, no effort has been made here to relate the roughness of the interface to its ability to reflect seismic energy.

The predicted seismic variations are given in Figure 5.5. These show that the variations in wavespeed are comparable to those of model RFM (Figure 5.3). Figure 5.1 (orange curves) shows the RMS-variations and values for R for model LIN after 4.5 Gyr. Due to the increased entrainment of deep mantle material, the values at depths between 700 and 2000 km are larger than in the reference model. Furthermore, the peak values in the RMS-amplitudes are shifted towards the CMB.

5.4 Wavespeed variations in model D0

Finally, the seismic wavespeed variations were calculated for model D0. Figure 5.7 shows the temperature and compositional variations and the associated seismic velocity variations are given in Figure 5.8. The RMS-amplitudes and R -values for model D0 are given by the blue curves in Figure 5.1. In the absence of the deep mantle reservoir, no compositional effects are present, as is indicated by the straight R -profile. Moreover, since convection is no longer layered, temperature variations in the lowermost mantle are also lower than in the reference model. Therefore, the absolute values for the RMS-amplitudes have significantly decreased. Variations in P- and S-wavespeed are now of the order of 0.5 and 0.75%, respectively.

These variations in model D0 are in good agreement with the seismological data (Figure 5.6). In contrast with this, the wavespeed variations in models RFM and LIN were a few times too large. This shows that the large temperature variations ($\sim 1000^\circ\text{C}$), that are accompanied by compositional mantle layering, lead to unrealistically large variations in the seismic velocity field. The match with seismological data improves when the compositional layering is omitted.

Although model D0 gives a better fit to the observed variations in P- and S-wavespeed, the constant value for R does not resemble the seismological data of R , which increases with depth. However, the result calculated here, is biased by neglecting the pressure dependence of the seismic derivatives, which affects the value of R directly.

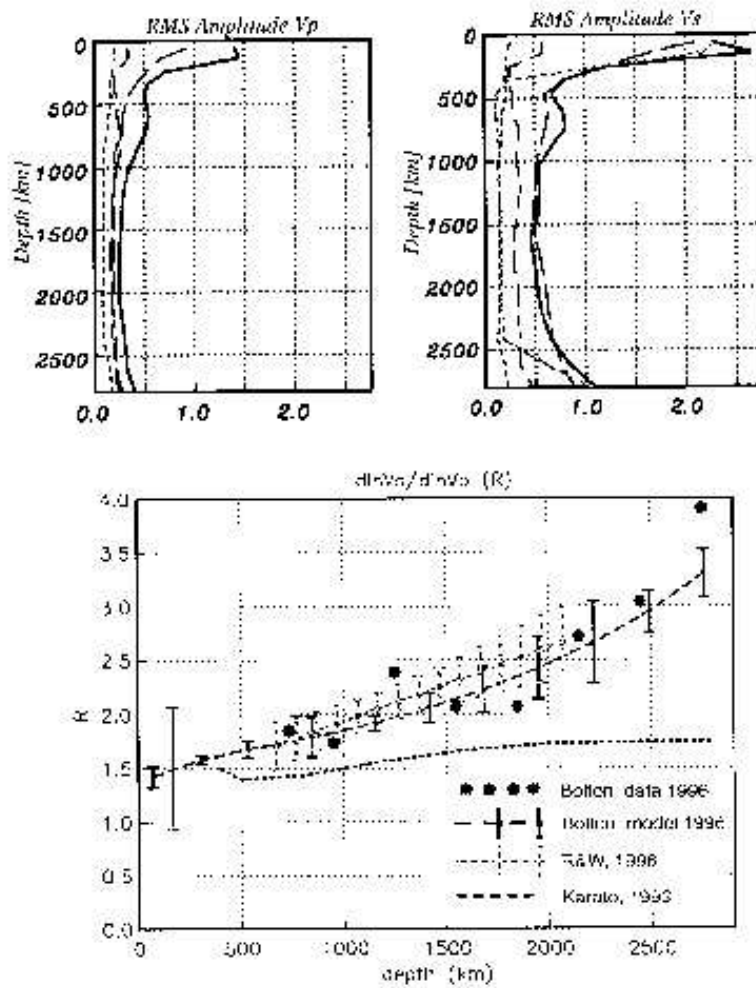


Figure 5.6: Overview of RMS-amplitudes and R values with depth from Masters e.a. (2000).

5.5 Conclusions

The predicted wavespeed variations lead to the following conclusions:

- In the reference model, the lateral lower mantle seismic perturbations are in the order of 1.5 and 2.5% for P- and S-wave velocities respectively. These variations are mainly caused by temperature variations, and to a lesser extent by compositional variations. When compared to the seismic data given in Masters and Laske (2000), these seismic variations are about four times too large.
- In model LIN, the sharpness of an initial gradient in the composition distribution increases with time. Still, after 4.5 Gyr, the interface is more gradual than in the reference model. This roughness is expected to reflect less detectable seismic energy. Furthermore, the compositional interface also shows an enhanced topography to the other models, because the volume averaged excess density of the deep mantle reservoir is lower than in the reference model.
- The mismatch between the RMS-amplitudes of model RFM and LIN and the seismological data given in Masters and Laske (2000), is caused by large lateral temperature variations, that are accompanied by compositional layering in the deep mantle. The match with the observations is improved substantially in model D0, where the compositional layering was removed.

Chapter 6

Discussion

In any model, the set of processes to describe reality is never complete. Approximations made in processes that are included, lead to errors in the model results. Additional errors are introduced by making use of numerical methods. These shortcomings and their effects will be discussed in Section 6.2 and 6.2. In Section 6.3 the results are related to recent speculations on the evolution and the present-day state of the Earth.

6.1 Approximations in the theoretical framework

The theoretical framework of extended-Boussinesq assumptions includes temperature- and depth-dependent viscosity and depth-dependent thermal expansivity. These are important improvements on the Boussinesq model as was shown in the study of Hansen and Yuen (2000). The model can further be improved by using the anelastic framework, which includes finite compressibility.

This research shows that the inclusion of the 660-km phase transition is crucial in simulating the mantle evolution, since it controls mass transport between the upper and lower mantle. The 410-km exothermic phase transition is believed to be less important. It was left out to prevent an unnecessary complicated analyses.

The thermal coupling between the mantle and core is more realistic than a zero heat flux or constant temperature boundary at the CMB. Its primary effect is a faster heating of cold slabs reaching the CMB, decreasing their residence time. The thermal coupling model would become even more realistic if radioactivity and latent heat production in the core were incorporated.

The temperature-dependence of the viscosity, produces a first order approximation of the complicated process of subduction. The viscosity profile was chosen pragmatically, to obtain realistic cooling rates and mantle velocities. Larger viscosity values would lead to a more rigid style of upper mantle convection. The upper mantle viscosities are in the range of values $10^{21} - 10^{22}$, which are in reasonable agreement with values for the upper mantle. The rheological model might further be improved by using a separate viscosity parameterisation in the upper and lower mantle and by using composition dependent viscosity.

Except for the deep mantle layer, chemical heterogeneity is lacking. Therefore, the thermally insulating effect of continents is missing, which could explain the large surface heat flux found in

the numerical results. Also, the model does not account for segregation of subducted oceanic crust, which may be important in the dynamic evolution of the mantle (Christensen and Hofmann (1994)).

Predictions of seismic velocity variations in Chapter 5 should be interpreted with care. In the seismic derivatives the pressure-dependency is not accounted for. Also, uncertainties in the seismic derivatives are large, especially for composition. The reliability of the predicted wavespeed variations can be improved when more constrained data for the seismic derivatives becomes available, and by including the pressure dependence of the derivatives. Finally, the D''-layer, which is expected to affect the seismic signature in the lowermost mantle, should also be incorporated.

6.2 Numerical approximations

In relation to the 3-D, spherical mantle, the volume-to-surface ratio of the mantle is exaggerated in the 2-D, cartesian model with a factor 1.6. Likewise, the heat production is overestimated with the same amount. In order to reduce the introduced errors, the heat production was scaled with a value 0.614. Model SCLD shows that this scaling is indeed important and should not be neglected. Another consequence of the cartesian geometry, is the overestimation of the CMB-surface area with a factor 3.4. For this effect, a correction was applied in the thermal coupling with the core. In spite of these two corrections, the convective behaviour in the mantle is most likely influenced by the 2-D, rectangular geometry (see e.g. Tackley (2002)). Therefore, 3-D, or at least 2-D, cylindrical models are recommended.

For the aspect ratio, values larger than 2.5 are desired in order to reduce the non-physical effects from the side boundaries. Another interesting option, less demanding on computational power, is the use of periodic boundary conditions. In this method, tracers crossing one side boundary are replaced on the other.

Although not reported, a benchmark on the effects of tracer density and element size was performed. The numerical errors introduced are believed not to undermine the stability of the results significantly.

6.3 Discussion of the model results

Presently, the nature of mantle dynamics is under debate and the model of compositionally layered convection is competing with other models. For this reason, it is important to search for evidence, which either proves or rejects the model.

This study shows that long-term compositional layering is dynamically feasible, which is in accordance with previous numerical modelling studies of Kellogg et al. (1999), Hansen and Yuen (2000) and Tackley (2002). In the models presented, compositional layering with substantial topography was found stable over a time period of 4.5 Gyr for an excess compositional density of $\sim 1.5\%$. The stability of the layering is most sensitive to variations in the excess compositional density, which is a model-dependent quantity.

The transition from layered to non-layered convection, has important consequences for the dynamic regime in the mantle. After this transition, the mantle cools faster, which is important in relation

to thermal evolution models. The timing of the transition is model-dependent, where a key role is played by the strength of the 660-km phase transition, which is relatively well constrained. Another important aspect in this light is the rheological model, since stronger slabs will cross the phase transition more easily and the transition will appear earlier in the Earth's evolution.

Although dynamically feasible, the model of layered convection must also explain a) the unsuccessful search for a sharp chemical boundary in seismological observations and b) the origin of the deep mantle reservoir.

To explain the unsuccessful search for seismic reflections, without having to reject the model altogether, seismic reflections must be hard to detect. This could be caused by a gradual chemical interface or large topography. Firstly, a gradual interface is favoured by defining a gradual, instead of a sharp, compositional transition initially. The sharpness of the transition may also be reduced by the effects of chemical reactions and chemical diffusion, although these effects were not examined. Secondly, a large topography is easily produced by adjusting the excess chemical density of the deep mantle reservoir close to the limit for unstable layering.

This study does not give a conclusive answer to what the conditions of the early Earth were, or what the origin of an enriched dense layer could have been. A magma ocean, core-mantle interactions, eclogite recycling, or a combination of any of these mechanisms are all possible. More work is definitely needed to show which of these options is most likely.

The seismic wavespeed variations, predicted in this study, are not in favour of the model of compositional mantle layering. They indicate wavespeed variations, caused by the temperature variations that are accompanied by compositional layering, are significantly larger than the observed seismological data suggests. The match with the data improves substantially when compositional layering is removed. However, as was explained in Section 6.1, the method used to calculate the seismic variations suffers from some simplifications and therefore, the predicted wavespeeds are not qualified as conclusive evidence against the model of compositionally layering. Still, the method of seismic wavespeed predictions gives relevant information and an additional test to the numerical model.

Chapter 7

Conclusion

In the introduction of this report, three research questions were formulated. After having presented and discussed the numerical results, these questions are answered here. This results in the three conclusions of this study.

1. *Is compositionally layered mantle convection stable in a cooling mantle over a period of time comparable to the age of the Earth, i.e. 4.5 Gyr?*

Yes, by adjusting the compositional excess density in the deep mantle reservoir, long-term stability can be reached. In this work, stability accompanied with large topography on a time scale of 4.5 Gyr was found stable for an excess density around 1.5%, which corresponds to a surface buoyancy number of $B_0 = 0.19$. This result has not been shown before, for a model including a phase transition or thermal coupling with the core.

The phase transition plays a crucial role in the transition from the layered to the non-layered convection regime and in the amount of material flux between upper and lower mantle afterwards. Heat from the core decreases the residence time of cold subducted slabs that reach the lowermost mantle.

2. *To what extent do the chosen parameter values relate to values for the real Earth?*

The initial model conditions are considered realistic for the early mantle, although large uncertainties remain in these conditions early in the Earth's evolution. After 4.5 Gyr model time, mantle temperatures, surface heat flow and the viscosity field are well comparable to the present-day Earth values. The jump in the heat flux across the CMB, associated with the transition from layered to non-layered convection is not in disagreement with paleomagnetic studies.

3. *How sensitive is the model to variations in the model set-up?*

The dynamic behaviour of layered mantle convection models is robust, for the parameter space examined. The transition from layered to non-layered convection around 2 Gyr is observed in all of the models that were examined.

The five most important conclusions from the parameter test result in Chapter 4 and 5 are listed below.

- The stability of compositional layering is model-dependent. The negative compositional buoyancy force, can be adjusted by varying the extra density in the deep mantle reservoir. The positive thermal buoyancy depends on the temperature difference between the mid- and deep mantle. This temperature difference is primarily controlled by the different cooling rates of the mantle reservoirs. The distribution of radioactive heat production is less important.
- The deep layer thermally blankets the core, not only by means of its enlarged heat production, but even more by limiting the contact between the hot core and the cold convective downwellings.
- The thermal coupling with the core heats the slabs that have reached the CMB, thereby increasing their mobility and decreasing their residence time in the deep mantle.
- When using 2-D, cartesian models, the volume of the mantle is overestimated by a factor 1.6. Therefore, scaling the volume integrated radioactivity is important when models are to be interpreted quantitatively.
- The predicted seismic velocity variations are on the high side when compared to seismological observations. These large values result from lateral temperature differences that are associated with compositional layering in the deep mantle. When the compositional layer is removed, the match with the seismological data improves.

Chapter 8

Acknowledgements

This research project would not have been possible without the help of other people. I therefore would like to thank everyone who helped me with the realisation of this project and all family and friends for making it a pleasant time altogether. The following persons I would like to mention specifically. My supervisor Arie van den Berg, for being helpful and supportive in many ways. Peter van Thienen for helping me out when my computer was being uncooperative. Rob van der Hilst for the discussions on seismology. Geert Strik for giving a useful update on paleomagnetism. All other staff members and students at University that I had scientific discussions with or just a cup of coffee or a game of chess to break the many hours of modelling work. My parents, for giving me the opportunity to study in the first place and my two brothers, for giving helpful comments every now and then.

Bibliography

- Abe, Y. (1996). Thermal and chemical evolution of the terrestrial magma ocean. *Physics of the Earth and planetary interiors*, 100:27–39.
- Albarede, F. (2002). Geochemistry.
- Albarede, F. and Van der Hilst, R. (2002). Zoned mantle convection. *Phil. Trans. R. Soc. Lond. A*, 360:2569–2592.
- Buffett, A. (2000). Dynamics of the earth’s core. *Geophysical Monograph: Earth’s Deep Interior*, 117:37–62.
- Castle, J. and Van der Hilst, R. (2000). Seismic observations of deep mantle structures. *Geophysical Research Letters*.
- Christensen, U. and Hofmann, A. (1994). Segregation of subducted oceanic crust in the convecting mantle. *Science*, 99:19,867–19,884.
- Davaille, A. (1999). Simultaneous generation of hotspots and superswells by convection in a heterogeneous planetary mantle. *Nature*, 402:756–760.
- Ekstrom, G. and Dziewonski, A. (1998). The unique anisotropy of the pacific upper mantle. *Nature*, 394:168–172.
- Forte, A. and Mitrovica, J. (2001). Deep-mantle high-viscosity flow and thermochemical structure inferred from seismic and geodynamic data. *Nature*, 410:1049–1056.
- Grand, S., Van der Hilst, R., and Widiyantoro, S. (1997). Global seismic tomography: a snapshot of convection in the earth. *Geol. Soc. Am. Today*, 7:1–7.
- Hansen, U. and Yuen, D. (2000). Extended-boussinesq thermal-chemical convection with moving heat sources and variable viscosity. *Earth and Planetary Science Letters*, 176:401–411.
- Hofmann, A. (1997). Mantle geochemistry: the message from oceanic volcanism. *Nature*, 385:219–229.
- Honda, S. (1995). A simple parameterized model of the earth’s thermal history with the transition from layered to whole mantle convection. *Earth and Planetary Science Letters*, 131:357–369.
- Irifune, T. and Ringwood, A. (1993). Phase transformations in subducted oceanic crust and buoyancy relationships at depths of 600-800 km in the mantle. *Earth and Planetary Science Letters*, 117:101–110.

- Jeanloz, R. and Lay, T. (1993). The core-mantle boundary. *Scientific American*, May:26–33.
- Kellogg, L., Hager, B., and Van der Hilst, R. (1999). Compositional stratification in the deep mantle. *Science*, 283:1881–1884.
- Larson, R. (1991). Geological consequences of superplumes. *Geology*, 19:963–966.
- Loper, D. and Lay, T. (1995). The core-mantle boundary region. *Journal of Geophysical Research*, 100(B4):6397–6420.
- Masters, G. and Laske, G. (2000). The relative behavior of shear velocity, bulk sound speed and compressional velocity in the mantle: Implications for chemical and thermal structure. *Geophysical Monograph: Earth's Deep Interior*, 117:63–87.
- Richter, F. (1985). Models for the archaic thermal regime. *Earth and Planetary Science Letters*, 73:350–360.
- Segal, A. and Praagman, N. (2000). The sepran package, technical report. <http://dutita0.twi.tudelft.nl/sepran/sepran.html>.
- Steinbach, V., Yuen, D., and Zhao, W. (1993). Instabilities from phase transitions and the timescales of mantle thermal evolution. *Geophysical Research Letters*, 20(12):1119–1122.
- Sumita, I., Hatakeyama, T., Yoshihara, A., and Hamano, Y. (2001). Paleomagnetism of late archaic rocks of hamersley basin, western australia and the paleointensity at early proterozoic. *Physics of the earth and Planetary Interiors*, 128(1-4):223–241.
- Tackley, P. (2002). Strong heterogeneity caused by deep mantle layering. *Geochemistry Geophysics Geosystems*, 3(4):1–22.
- Trampert, J., Vacher, P., and Vlaar, N. (2001). Sensitivities of seismic velocities to temperature, pressure and composition in the lower mantle. *Physics of the Earth and Planetary Interiors*, 124:255–267.
- Turcotte, D., Paul, D., and White, W. (2001). Thorium-uranium systematics require layered mantle convection. *Journal of Geophysical Research*, 108:4265–4276.
- Van den Berg, A. (2000). Numeriek modelleren van geodynamische processen. 3.
- Van den Berg, A., Van Keken, P., and Yuen, D. (1993). The effects of a composite non-newtonian and newtonian rheology on mantle convection. *Geophys. J. Int.*, 115:62–78.
- Van den Berg, A. and Vlaar, N. (2001). Warmtetransport in de aarde. 21.
- Van der Hilst, R. and Karason, K. (1999). Compositional heterogeneity in the bottom 1000 kilometers of the earth's mantle: Toward a hybrid convection model. *Science*, 283:1885–1888.
- Van der Hilst, R.D. and Widiyantoro, S. and Engdahl, E. (1997). Evidence for deep mantle circulation from global tomography. *Nature*, 386:578–584.
- Van Hunen, J. (2001). Shallow and buoyant lithospheric subduction: causes and implications from thermo-chemical numerical modelling. *Geologica Ultraiectina*, 211.

- Van Thienen, P., Van den Berg, A., De Smet, J., Van Hunen, J., and Drury, M. (in press). The interaction between small scale mantle diapirs and a continental root. *Geochemistry Geophysics and Geosystems*.
- Vidale, J. and Schubert, G. (2001). Unsuccessful initial search for a midmantle chemical boundary with seismic arrays. *Geophysical Research Letters*, 28:859–862.
- Vlaar, N., Van Keken, P., and Van den Berg, A. (1994). Cooling of the earth in the archaean: consequences of pressure-release melting in a hotter mantle. *Earth and Planetary Science Letters*, 121:1–18.

Appendix A

Thermal Coupling of the Earth's Mantle and Core

Initially, the core temperature is set to the value T_{core}^0 . The change in core temperature ΔT_{core}^i is calculated after each time step from the conductive heat exchange between the core and the mantle. The core is assumed to be a uniform reservoir without heat production. So:

$$\Delta T_{core}^i = \frac{\langle q \rangle^i A \Delta t^i}{C_{core}} \quad (\text{A.1})$$

where $\langle q \rangle^i$ is the mean heat flow density across the CMB during a time step Δt^i . C_{core} is the core heat capacity, which is equal to $\rho_{core} c_{P,core} V_{core}$. The core heat capacity is taken as a constant fraction of the mantle heat capacity. This fraction is denoted by f . So:

$$C_{core} = f C_{man} \quad (\text{A.2})$$

with

$$f = \frac{(\rho c_P V / A)_{core}}{(\rho c_P V / A)_{man}} \quad (\text{A.3})$$

The values for the volume V and surface A are calculated for the spherical Earth. In this way, the overestimation of the volume and surface in a 2-D, cartesian geometry was reduced. The ratio of the Earth's radius to the core radius was taken as 1.833. Then, using $\frac{\rho_{core}}{\rho_{man}} = 2.3$, $\frac{c_{P,core}}{c_{P,man}} = 0.64$, $\frac{V_{core}}{V_{man}} = 0.162$ and $\frac{A_{man}}{A_{core}} = 3.361$, we get a value of 0.8 for f .

At the end of time step i , the new temperature of the core T_{core}^{i+1} , is calculated using:

$$T_{core}^{i+1} = T_{core}^i - \Delta T_{core}^i \quad (\text{A.4})$$

Finally, the temperature of the bottom boundary of the mantle is set equal to this new core temperature before a new time step is started. This process is repeated in every timestep.

Appendix B

Calculation of a time-dependent buoyancy number and entrainment

A post-processing FORTRAN-program was written in order to quantify a) a time-dependent buoyancy number $B(t)$ and b) the entrainment of the deep reservoir material into the upper mantle, denoted ENT .

B.1 Quantifying a time dependent buoyancy number

In order to calculate the entrainment ENT and buoyancy ratio $B(t)$, it is necessary to distinguish between enriched and depleted material. To this end, the composition, temperature and viscosity fields were interpolated to an evenly spaced grid as a basis for post-processing. Gridpoints with a composition value larger than 0.5 were identified as enriched material. Gridpoints with lower composition values were identified as depleted mantle material. After having made this distinction, it is possible to calculate mean values for the quantities temperature, composition and viscosity for both the enriched and the depleted material separately.

The temperature difference between the enriched and the depleted mantle, was used to calculate a time dependent value for the buoyancy number $B(t)$ as follows:

$$B(t) = \frac{1}{\alpha_0(T_{dm}(t) - T_{umm}(t))} \frac{\delta\rho}{\rho_0} \quad (\text{B.1})$$

B.2 Quantifying the entrainment of deep mantle reservoir material

To calculate the entrainment, first, the excess composition for both layers was calculated. This was done by adding all composition values exceeding 0 for both layers, giving a quantity C_{umm} and C_{dm} . The entrainment ENT was calculated as the excess composition of the upper and mid-mantle divided by the total excess composition:

$$ENT = \frac{C_{umm}}{C_{umm} + C_{dm}} \quad (\text{B.2})$$

Appendix C

Calculation of Seismic Velocity Anomalies

A FORTRAN program 'seismo' was written to translate absolute compositional density perturbations ($\delta\rho_c$) and absolute temperature perturbations (δT) into relative perturbations of seismic velocity ($\delta \ln v$). With relative perturbation, the percentual difference from the horizontal mean value is meant. We thus want to calculate:

$$\partial \ln v = \frac{\partial \ln v}{\partial T} \delta T + \frac{\partial \ln v}{\partial \rho_c} \delta \rho_c \quad (\text{C.1})$$

C.1 Calculating temperature and compositional density perturbations

δT and $\delta \rho_c$ can be calculated directly from the SEPRAN output data. The temperature and compositional fields, are read from P3-files, containing an n_x by n_y -sized list of values for every point (i,j). First the horizontal average of a quantity q is calculated for every row j , giving \bar{q}_j .

$$\bar{q}_j = \frac{1}{n_x} \sum_{i=1}^{n_x} q_{ij} \quad (\text{C.2})$$

The perturbation with respect to the horizontal average is then calculated for all field points as:

$$\delta q_{ij} = q_{ij} - \bar{q}_j \quad (\text{C.3})$$

The operations above are executed for both the temperature field T_{ij} and the compositional density field $\rho_{c,ij}$. The compositional density field was calculated straightforward from the compositional field, using $\rho_{ij} = 1 + C_{ij} \frac{\delta \rho}{\rho_0}$. With C_{ij} the composition and $\frac{\delta \rho}{\rho_0}$ the excess density of the enriched material.

C.2 Dependence of velocity on temperature and composition

Values for $\frac{\partial \ln v}{\partial \rho_c}$ and $\frac{\partial \ln v}{\partial X}$ were deduced from the work of Trampert et al. (2001) and are listed in Table 5.1. X is the molar fraction of a certain element.

To calculate the seismic wavespeed variation, equation (C.1) first has to be rewritten as

$$\partial \ln v = \frac{\partial \ln v}{\partial T} \delta T + \frac{\partial \ln v}{\partial X} \frac{\partial X}{\partial \ln \rho_c} \delta \rho_c \quad (\text{C.4})$$

Then, using $\frac{\partial \rho_c}{\partial X} = 0.2$, we have all the information to calculate $\partial \ln v$ from δT and $\delta \rho_c$.

Appendix D

Modelling Density Variations in an Incompressible Flow Model Using a Penalty Function Approach

During this study, a practical problem was encountered, causing severe non-physical effects in the model results. It was observed that for models on a Gyr time scale, the flow field is not divergence-free, as it should be in the extended-Boussinesq approximation (see Section 2.1). This may result for instance in the violation of conservation of volume of the dense enriched layer on a long time scale.

In the finite element part of the convection code, the divergence of the flow field in equation 2.9 and the pressure gradient in equation 2.10 are coupled, using a penalty function term ϵ :

$$\Delta p = \frac{1}{\epsilon} \nabla \cdot \vec{u} \tag{D.1}$$

This approximation to equation 2.9 is used to eliminate the pressure gradient from the Stokes equation (equation 2.10). The reference value for ϵ used in the code is 1.10^{-6} . Apparently, this small value is still too large for models where, on a Gyr time scale effects of small divergences can add up and introduce non-physical effects such as the compaction and expansion of layers with contrasting density. An example is shown in Figure D.1 where the most dense concentration of tracer particles represent the deep mantle material. Obviously the volume of the deep layer does not remain constant, but decreases with time. The amount of compaction is illustrated in Figure D.2.

A practical solution was found by subsequently decreasing ϵ by a factor 10 in the range 1.10^{-6} - 1.10^{-9} . The distribution of tracers in Figure D.1 shows that the divergence associated with density jumps practically vanishes for $\epsilon = 1.10^{-9}$. The local low-density zones in the tracer distribution are not steady, and therefore less worrying. Figure D.2 also shows that the compaction of the deep mantle disappears for smaller ϵ .

Thus, a lowering of ϵ appears to be an effective remedy against the undesired non-physical compaction. Still, ϵ cannot be taken infinitely small, since it would introduce truncation errors in the numerical results. These truncation errors would be associated with a divergent solution. To check